DESIGN OF NEXT GENERATION STATIONARY DIGITAL BREAST TOMOSYNTHESIS SYSTEM

Tuyen Phan

A thesis submitted to the faculty of the University of North Carolina at Chapel Hill in partial fulfillment of the requirements for the degree of Master of Science in the Department of Biomedical engineering.

Chapel Hill
2010

Approved by:

Dr. Otto Zhou

Dr. David Lalush

Dr. Marija Ivanovic

Dr. Jianping Lu

ABSTRACT

TUYEN PHAN: Design of Next Generation Stationary Digital Breast Tomosynthesis System
(Under the direction of Dr. Otto Zhou)

Digital breast tomosynthesis is a three-dimensional mammography technique where scans are acquired at a limited angle and the projections are reconstructed. It overcomes the main limitation of mammography, which is tissue overlap, by providing improved depth resolution. The emerging technology still uses a conventional x-ray source based on thermionic emission that requires rotation of the source to cover the angular range.

This thesis presents the design and characterization of a next generation stationary digital breast tomosynthesis system that uses a carbon nanotube-based (CNT-based) multi-pixel x-ray source. The CNT-based x-ray source eliminates the need for rotation of the x-ray tube and allows for higher temporal resolution because the pixels can be switched on instantaneously. The system will be able to operate at 30-60 kV and can be used for quasi-monochromatic imaging at a reasonable scan time in order to increase contrast between tissues of similar attenuation.

TABLE OF CONTENTS

LIST OF TABLES

Table

LIST OF FIGURES

Figure

CHAPTER 1

INTRODUCTION

Breast cancer is the second leading cause of cancer death among women, preceded only by lung cancer. In 2009, 192,370 new cases of invasive breast cancer were diagnosed in the United States and 40,170 deaths resulted from it. There is a 13% chance that a woman will develop invasive breast cancer some time in her life and a 3% chance that it will result in her death.[1] In the past decade, the death rate has been declining due in part to early detection through screening. Mammography is currently the most effective tool for early detection of breast cancer. However, limitations still exist with conventional mammography. Digital breast tomosynthesis, an emerging technology, will address some of those issues. The thesis focuses on a stationary digital breast tomosynthesis system for 3D breast cancer imaging.

CHAPTER 2

BACKGROUND

2.1 History of Conventional Mammography and its Limitations

Breast imaging can be traced back to the surgeon Albert Salomon, who in 1913 used radiography of mastectomy specimens to show the spread of tumor to the axillary lymph nodes. In 1960, Robert Egan described a mammographic technique using high current, low voltage, and film that could easily be reproduced. He was able to demonstrate excellent results in his first 1000 patients, which lead to the widespread use of mammography. In 1965, Charles Gros along with the CGR Company (Compagnie Générale de Radiologie) developed the Senographe, the first prototype dedicated mammography unit (Fig. 1). Shortly after, in 1973, DuPont developed a device to hold the screen and film together by creating a vacuum. Prior to this, mammograms required hand processing or the use of a slow mechanical processor. DuPont became the first company to market a dedicated screen-film mammography system. [2]

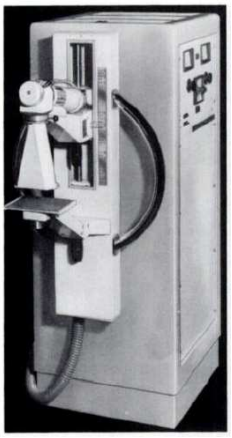

Figure 1: Prototype of the Senographe

Conventional screen-film mammography is a two-dimensional imaging modality where x-rays are absorbed onto a fluorescent screen and the emitted light is recorded on photographic film. The typical x-ray tube used (Fig. 2) consists of a cathode, usually a W filament, which when heated to a high temperature, emits electrons. The electrons are accelerated by an anode voltage and bombards the target, usually W or Mo. The kinetic energy lost at the anode is converted to x-rays and are emitted perpendicular to the path of the electron current.[3]

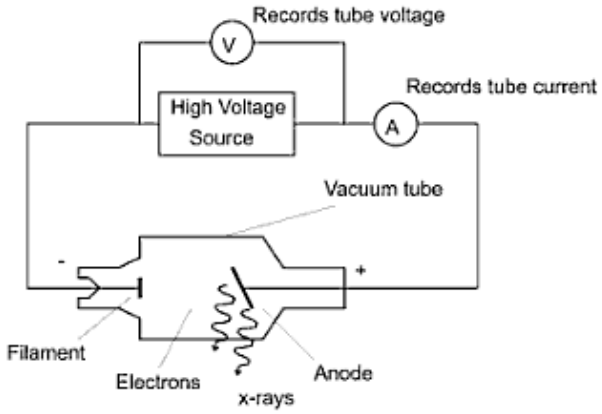

Figure 2: Typical x-ray tube

There are two types of radiation produced: Bremsstrahlung radiation and characteristic x-rays. Bremsstrahlung radiation is a result of the deceleration of electrons by the nucleus of the target material and is characterized by a continuous distribution of x-rays. Characteristic x-rays, on the other hand, are produced when an L shell electron transitions to the K shell to fill the hole left after an electron is ejected by a high kinetic energy electron. [4] They are seen as peaks at certain photon energies in the x-ray spectrum (Fig. 3) and the energies of the peaks produced depend on the target material used.

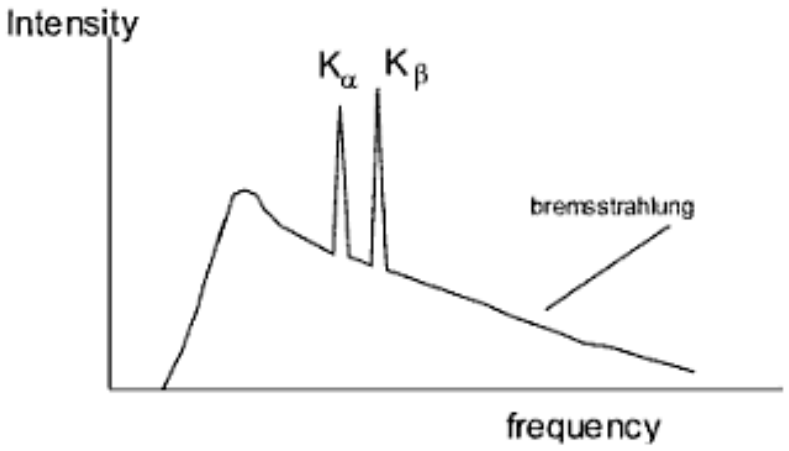

Figure 3: Typical x-ray spectrum

In mammography, the images of the compressed breast are acquired in two views, cranial-caudal (CC) or head-to-toe and mediolateral oblique (MLO) or at a 45° angle. Digital mammography is similar to conventional mammography except a digital detector is used to produce computerized images. This allows for the brightness and contrast of the images to be adjusted. There is no significant difference in cancer detection rate between screen-film and digital mammography. [5] However, screen-film mammography is less sensitive to cancers in women with radiographically dense breast. Sensitivity values range from 45% to 88%.[6] The main limitation of mammography is tissue overlap, which contributes to the very high false positive rate.

2.2 Digital Breast Tomosynthesis (DBT)

Digital breast tomosynthesis is a three-dimensional mammography technique, which has existed for over 30 years but is only recently being combined with digital mammography. Instead of acquiring images in only two views as done in mammography, scans are acquired at a limited angle to provide improved depth resolution. The x-ray tube is rotated along an arc by usually ±15 degrees in increments of 3° for a total of 11 views. [7] Like conventional mammography, the breast is slightly compressed and the detector remains stationary. Objects at different heights in the breast are projected differently onto the detector. In order to do the reconstruction, the projections are shifted relative to one another to enhance objects at different heights and the projections are summed as shown in figure 4. [8]

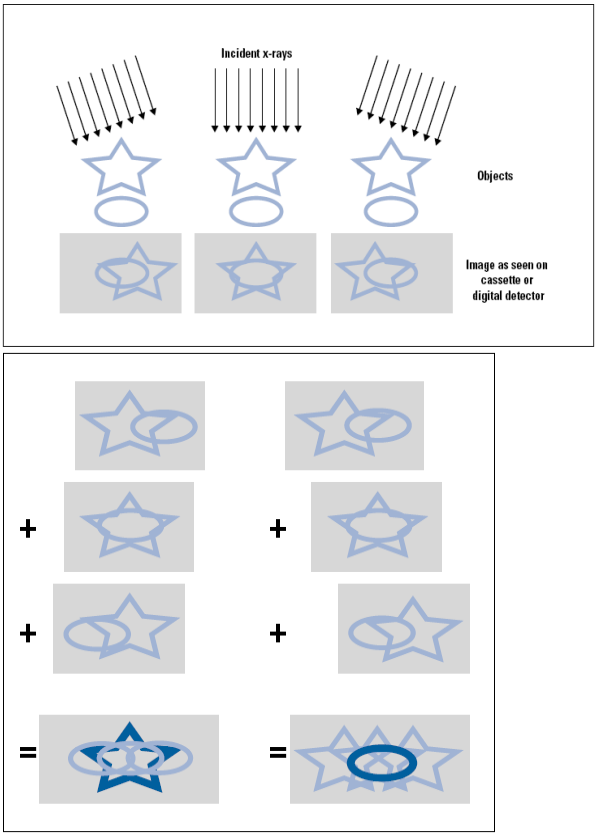

Figure 4: Tomosynthesis reconstruction whereby projections are shifted relative to one another and summed.

2.3 Carbon Nanotubes as a Field Emission X-ray Source

Carbon nanotubes (CNTs) were discovered in 1991 by Iijima. They can be classified into two categories: single-walled nanotubes (SWNTs) and multi-walled nanotubes (Fig. 5). SWNTs consist of a single graphite sheet rolled into a cylinder typically 1-50 nm in diameter and 1-10 μm in length. MWNTs consist of several graphite sheets rolled into a cylinder. [9] CNTs possess a unique structure and properties, which make them excellent field emitters.

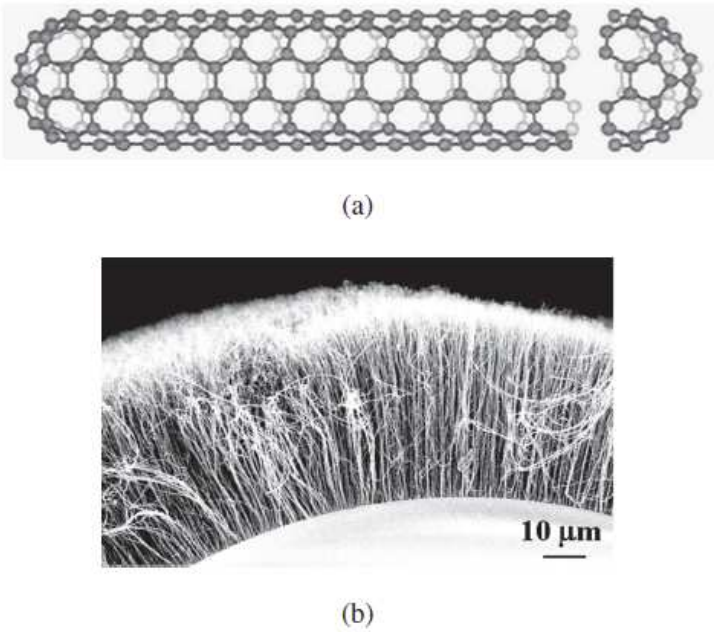

Figure 5: (a) Structure of a single-wall carbon nanotube; and (b) SEM image of multi-walled carbon nanotubes

In thermionic emission, the source, usually a W filament is heated to high temperatures of greater than 1000°C in order for its free electrons to possess enough thermal energy to overcome the surface potential barrier. The high temperature required results in energy loss so it is not a power efficient process. Unlike thermionic emission, field emission requires no heat. Instead, electrons are extracted from a conducting solid by an electric field. [10] The electric field narrows the electrons' potential barrier to vacuum so that electrons can quantum-mechanically tunnel through this solid-vacuum barrier. Field emission can be described using the Fowler-Nordheim (FN) model. The Fowler-Nordheim equation for the current emitted is given by: $I = AJ_{FN}$ where A is the emission area and J_{FN} is the current density. The Fowler-Nordheim equation for current density is given by: $J_{FN} = c_1F_1^2 \exp(-c_2\phi^{3/2} / F_t)$, where F_t is the electric field at the tip apex, ϕ is the work function, and c_1 and c_2 are constants. The electric field F_t can also be expressed as $F_t = \beta (V/d)$ where β is the field enhancement factor, V is the applied voltage, and d is the distance. The current density can be rewritten as follows: $J_{FN} = c_1(\beta V)^2 / \phi d^2 \exp(-c_2 d\phi^{3/2} / \beta V)$. [9] The FN model shows that to maximize current for a given applied voltage, the material used needs to have a low work function and be as sharp as possible in order to obtain the highest field enhancement factor. Figure 6 shows a typical Fowler-Nordheim plot. Using CNTs as the source, emission has been observed at electric fields as low as 1 V/μm and current densities of over 1 A/cm^2 have been obtained. [10]

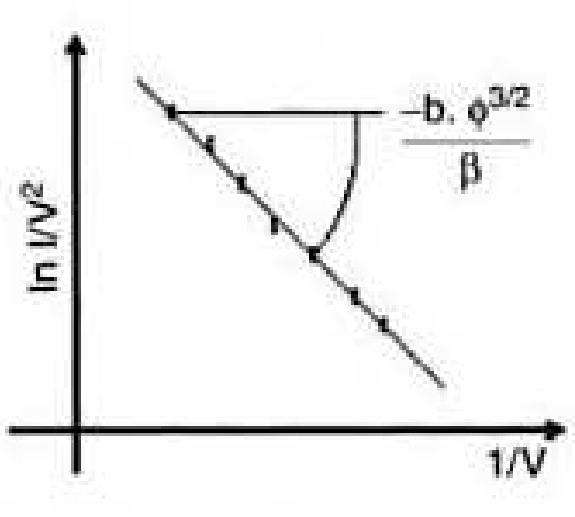

Figure 6: Typical Fowler-Nordheim plot

The use of CNT-based x-ray sources has been demonstrated in several applications. Among the applications is a single source micro-CT scanner for small animal imaging built in Dr. Otto Zhou's lab at the University of North Carolina at Chapel Hill. The stationary digital breast tomosynthesis system is an extension of that technology and uses a multi-pixel x-ray source for 3D breast cancer imaging. By applying an electric field between the cathode and gate electrode, the pixel can be switched on instantaneously. This allows for a multi-beam x-ray system with an array of pixels that can be switched on consecutively to cover the entire FOV and eliminate the need for tube rotation.

CHAPTER 3

DESIGN OF STATIONARY DIGITAL BREAST TOMOSYNTHESIS SYSTEM

3.1. Design Goals

The specific aims for the stationary digital breast tomosynthesis system is one that will be able to be used clinically and acquire images in both the cranio-caudal (CC) and medio-lateral oblique (MLO) views. Its performance will be comparable to a Siemens Mammomat Novation system. It will be able to operate at 30 kV to 60 kV for dual energy imaging and will have a tube current of up to 100 mA. The target effective FSS is 500 μm and the target total scan time is 3 s. This is feasible because of the use of a carbon nanotube-based (CNT-based) multi-beam field emission x-ray (MBFEX) source.

One advantage of a stationary DBT system over other DBT systems is that the CNT-based x-ray source allows for higher temporal resolution. With a higher temporal resolution, a faster scanning time can be achieved and motion blur reduced. Another advantage is that it is more stable than a step-and-shoot system because it does not require a rotating gantry. Moreover, unlike a system with continuous rotation where the x-ray effective focal spot size (FSS) is enlarged along the direction of motion, a stationary DBT system has a smaller effective focal spot size and hence better spatial resolution. This chapter will focus on the overall design for the system including designs for the array assembly, chamber, and mounting structure.

3.2 Design for Array Assembly

The stationary digital breast tomosynthesis system was designed to have a source-to-object distance of 64.5 cm and acquire twenty-five projection images, with each view separated by 2° for a total angular coverage of 48°. Each x-ray pixel (Fig. 7) consists of a CNT cathode, gate, focusing unit, and anode. The electron source is an 8 × 2 mm elliptical cathode made by XinNano using photolithography to define the elliptical shape and electrophoresis for CNT deposition on a 34 × 11mm glass substrate that is 2.8 mm thick. An Ag lining is printed on the glass substrate and acts as a conductor. Before the cathode can be used, it is activated with Kapton tape by taping it twice. The cathode is housed in a stainless steel holder with a groove to fix its position. Each cathode is insulated from the array holder and hence chamber by a 1.6 mm thick quartz plate. An ~180 μm thick mica spacer with a 10 mm opening is used to create a gap between the cathode and gate electrode. This distance determines the electric field between them.

The gate is 1 mm thick and has a 100 mesh woven from 0.0254 mm diameter W wires spot-welded onto the 10 mm opening to allow electrons to pass through. The focusing unit consists of two focusing electrodes based on Einzel lenses. The first focusing electrode, 6 mm thick, has a truncated cone with a cone angle of $2\tan^{-1}(1/2)$. Its purpose is to focus the diverging electrons coming out of the gating grid into a more parallel shape before they reach the second focusing electrode, which has a 10 mm opening and is 1 mm thick. The gate and focusing electrodes are made of stainless steel. Their thicknesses are important because FSS increases with increasing electrode thickness. However, the electrodes cannot be too thick as that may cause a decrease in electron transmission. In order to insulate the gate from the first focusing electrode and insulate the focusing electrodes from one another, 1 mm thick ceramic

washers are used. Four ceramic screws are used to fix the components of each x-ray pixel together onto an Al base. Counterbores are used to hide the screw heads and prevent arcing.

The anode is made of W and has a tilt angle of 16 degrees. It is fixed in a holder and separated from the second focusing electrode using two ceramic spacers. The distance between the anode and second focusing electrode is 9 mm. The anode holder is screwed to the spacers using vented stainless steel screws while the ceramic spacer is fixed to the Al base using vented stainless steel screws via a counterbore mechanism. Vented screws are used to allow trapped gasses to escape in order to acquire better vacuum conditions.

The twenty-five pixels are fixed onto an Al base and arranged at an angle so that the center of the cone beam for each pixel hits the center of the object to be imaged. Figure 8 shows the assembled array for every other pixel for a total of thirteen pixels. When the array is placed in the chamber, it has to be lifted up by using two Al plates placed underneath the Al base so that the x-ray beams align with the window of the chamber. The entire array is bolted to the chamber using two screws on each end of the Al base so that the assembly will be secure when it is mounted to the side of the chamber. This is done for operation at 30 kV. For operation at 60 kV, the two Al plates are removed and washers are added underneath the anode spacers to increase the distance between the anode and the second focusing electrode from 9 mm to 15 mm while keeping the x-ray beams aligned with the window. The distance between the anode and second focusing electrode was determined by assuming a 10 mm distance required for 40 kV tube voltage and a linear relationship. This distance is important as it affects the FSS. As the distance between the anode and second focusing decreases, the field gradient increases, thus contributing to the decrease in FSS. The distance is further critical in preventing arcing and dark current.

The connections for the electrodes are made using UHV compatible Kapton insulated wires that can be baked up to 250 °C. Additional insulation is provided with ceramic beads. To eliminate the need for soldering, the wires are wrapped around banana plugs that are threaded on the end and they are fixed with a nut. The electrodes for each pixel have holes where a banana plug can be inserted. The anodes for all the pixels are held at the same potential. One end is connected using a banana plug to a custom-made connector that is attached to a single pin feedthrough from Insulator Seal (part # 9442013). The feedthrough has a voltage rating of 60 kV and a current rating of 3 A. The gate and focusing electrodes are separately connected to a four pin feedthrough from MDC Vacuum Products (part # 634004). The feedthrough has a voltage rating of 5 kV DC and a current rating of 5 A. The electrodes have color-coded glass-ceramic beads attached at the end for identification purposes when making the connections to the feedthrough. The connections for the cathodes are made using a Kapton insulated ribbon cable. Each wire on one end of the ribbon cable is connected to a cathode via a stainless steel piece with a tiny clip attached that can be bent to connect directly to each cathode. The other end is connected to a 32-pin feedthrough from CeramTec via crimp contacts. The feedthrough has a voltage rating of 1 kV DC and a current rating of 5 A per pin.

Since the cathodes need to be kept under vacuum to keep them from oxidizing, which would decrease and destabilize the emission, it is important that all components placed in the chamber are chosen carefully. All of the materials placed in the chamber are either UHV compatible and/or have low outgassing rates. The cathode and anode holders, gate electrodes, and focusing units were electropolished with EPS2000 solution and sonicated in distilled water before being assembled. The W anode was cleaned with a solution containing

50 ml HNO3 + 30 ml H2SO4 + 20 ml distilled water for one to two minutes and rinsed with distilled water. It was annealed for an hour at 1000°C before being used in the assembly. The Al array holder was cleaned by soaking it in a 50/50 mixture of Oakite 33 and distilled water for two hours. The chamber, with the array assembled, can be baked up to 200 °C. Baking is a critical process in reversing the negative effects of oxidation on the field emission property. To prevent arcing and dark current, it is important to remove all sharp edges so the edges of some components were deburred.

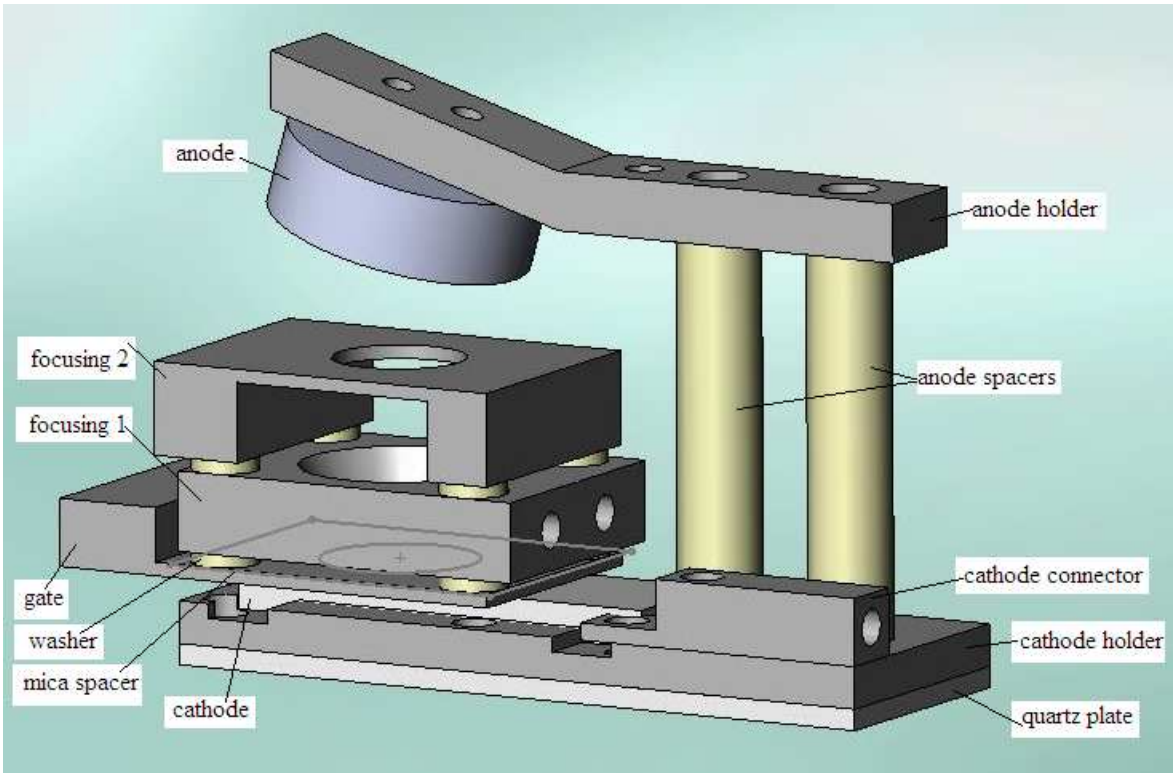

Figure 7: CAD drawing of an x-ray pixel

(a)

(b)

Figure 8: (a) Assembled array of thirteen pixels; and (b) close-up of assembled array

3.3 Design for System Chamber and Mounting Structure

The chamber that houses the assembled array was custom designed to be able to maintain a low vacuum pressure, at least 1.0×10^{-8} Torr, and be baked to a high enough temperature to reverse the process of oxidation. It is a 1041.4 × 120.1 × 120.1 mm (l × w × h) chamber with 3 mm thick walls made of stainless steel. It can accommodate two 8 inches flanges, one on each end. It also consists of four nipples in the back to accommodate four flanges. One 2.75 inches flange is for the cathode feedthrough and the other 2.75 inches flange is for the electrode feedthrough (gate and focusing unit). The 4.5 inches flange is for the high voltage feedthrough connected to the anode. The 2.75 inches flange in the center of the chamber is attached to a 4-way standard cross that connects to the vacuum gauge, ion pump, and gate valve. The gate valve is used to connect to the turbo pump and allows the pump to be removed when not in use by closing the valve. There is a stainless steel/aluminum plate welded onto the chamber with twenty-five rectangular Al windows, each 0.8 mm thick, to filter low energy x-rays. Siemens built the chamber and conducted a test by baking it to 320 °C for six hours.

The mounting structure was designed to securely support the chamber and make the system more clinical. The chamber can be rotated by +/- 45 °C by removing a quick-release pin so that images can be acquired in both the MLO and CC views (Figs. 9 and 10). A counterweight is placed on the mounting structure for easy rotation of the chamber and stops are put in place in order to prevent over-rotation. There are plates to hold a Varian Paxscan 2520 detector with dimensions of 6.17 × 27.9 × 25.8 cm (h × w × d) or one of comparable size. To accommodate a detector size, which varies greatly from that, only the plates need to be changed. The detector can be manually adjusted along the x, y, and z axes in order to

change the source-to-object distance and so that the center of the x-ray beam can hit the thickest part of the breast. It was also designed to be adjustable to accommodate varying size detectors with different size FOVs. A compression plate can easily be attached when needed.

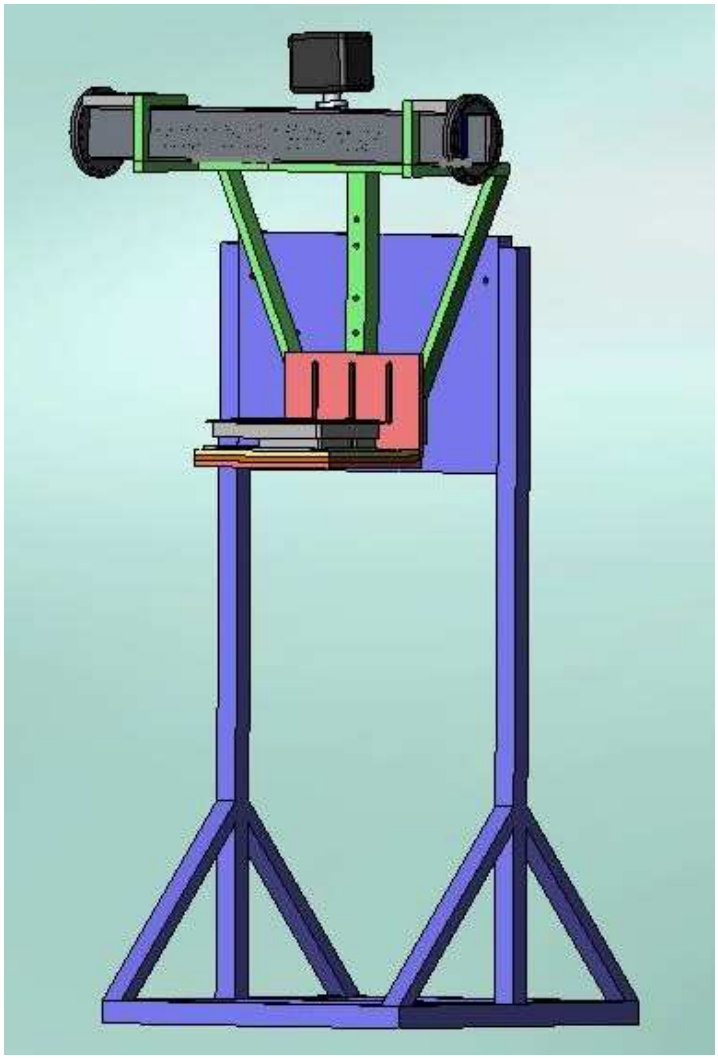

Figure 9: CAD drawing of the mounting structure

Figure 10: Mounting structure with chamber

3.4 Overall System Design

In order to generate x-rays, a voltage between 0 to 3 kV is applied between the cathode and gate electrode. Electrons are extracted as a result of the electric field created and the emitted electrons pass through the gate mesh. The electron beam passes through the focusing unit, with each focusing electrode held at a constant voltage between 0 to 2.5 kV. To determine the voltage for each focusing unit, a FSS measurement is performed and the voltages that give the optimal FSS for the pixels is used. The focused electron beam bombards the W anode and x-rays are generated. A 400 kΩ resistor is connected between the anode and high voltage power supply to protect the power supply in case of arcing. To control each pixel, a switching system is used that outputs a trigger signal. It acts like a MOSFET. In the low state, the source and drain would be closed in a MOSFET so the cathode is floating relative to ground and no electrons are emitted, hence no x-rays are generated. In the high state, the cathode is grounded so the electric field between the gate and cathode causes electrons to be emitted. A schematic diagram of the circuit is shown in figure 11. Since the current for each cathode varies from one another, manually adjustable resistors are used to compensate for the difference. [11]

The low vacuum needed is achieved by using a turbo pump and ion pump. The turbo pump is used to first pump down the system. Once a low enough pressure is reached, it is disconnected from the system by closing the gate valve. The ion pump is turned on to maintain the vacuum. When all twenty-five pixels are assembled and placed in the chamber, the vacuum has been able to go as low as 1.6×10^{-8} Torr after baking at ~170° C.

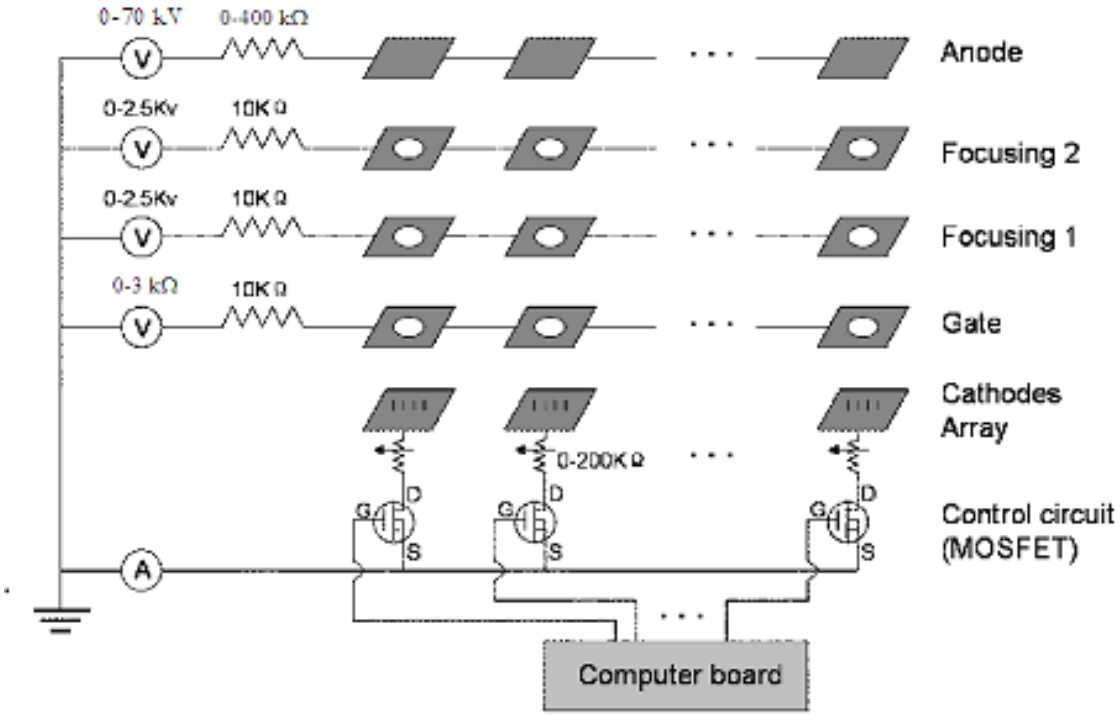

Figure 11: Schematic diagram of circuit

CHAPTER 4

SYSTEM CHARACTERIZATION

4.1 Diode Field Emission

In order to characterize the system, diode field emission data were acquired for the 8 × 2 mm cathodes. Figure 12 shows a plot of the field emission for thirty-four samples in the first batch of cathodes from Xinano. The measurements were recorded using 1% duty cycle (1 Hz, 10 ms), a 20 kΩ resistor, and 150 μm gap distance between the cathode and gate (which acted as the anode) created by using a microscope slide. The plot takes into account the resistance used. The variation in the turn-on field for thirty-one out of the thirty-four samples is ~2 V/μm. There are three cathodes that have slightly higher turn-on fields and this can depend either on the cathode property and/or how it is taped. Figure 13 shows the consistency over three runs and figure 14 shows the current density for sample 13. Figure 15 shows a plot of the field emission for eighteen samples from the second batch of cathodes from Xinano received about a year later. The measurements were recorded using 1 % duty cycle (1 Hz, 10 ms), a 10 kΩ resistor, and 150 μm gap distance between the cathode and gate. The plot takes into account the resistance used. With the exception of two cathodes, all of the cathodes are able to reach at least 40 mA in diode mode and the variation in the turn-on field is ~1 V/μm between the cathodes. The turn-on field remains fairly consistent

between the two batches of cathodes and is within 3-5 V/μm. The second batch has a narrower range for the turn-on field. This has to do with either the cathode property and/or how it is taped. Thus, careful taping of the samples is critical in getting good field emission.

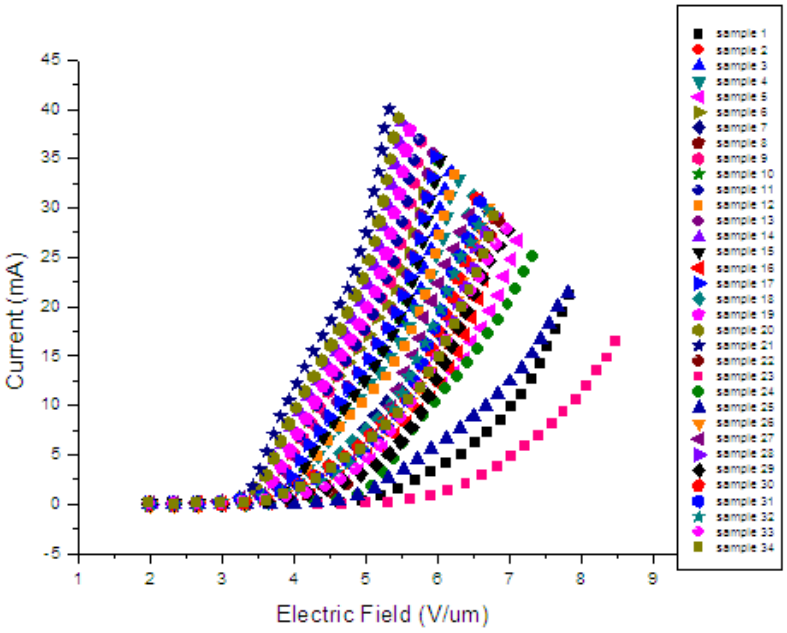

Figure 12: Current vs. electric field for thirty-four samples in first batch of cathodes

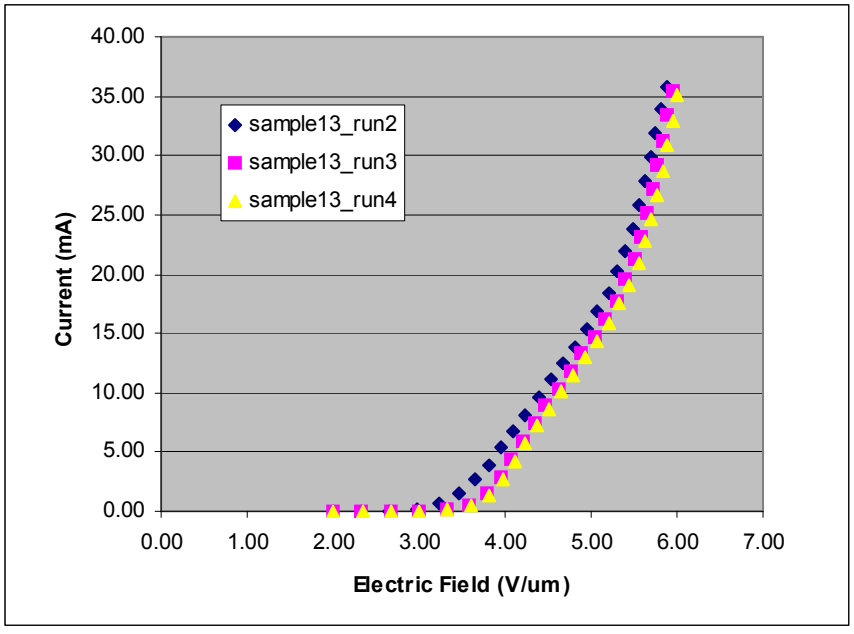

Figure 13: Current vs. electric field for sample 13 over three runs

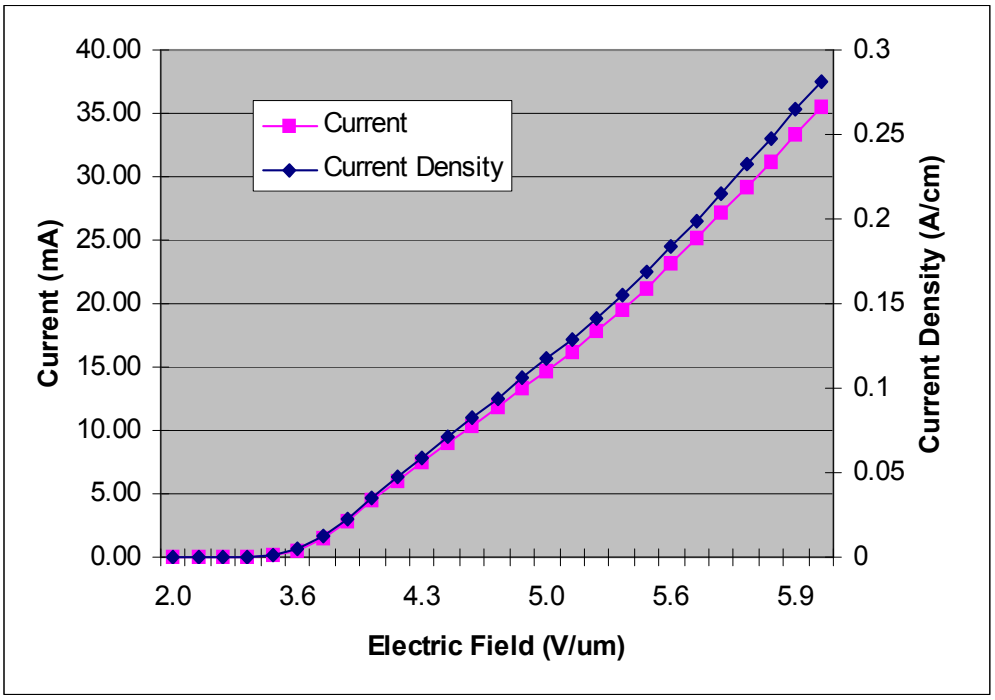

Figure 14: Current and current density vs. electric field for sample 13

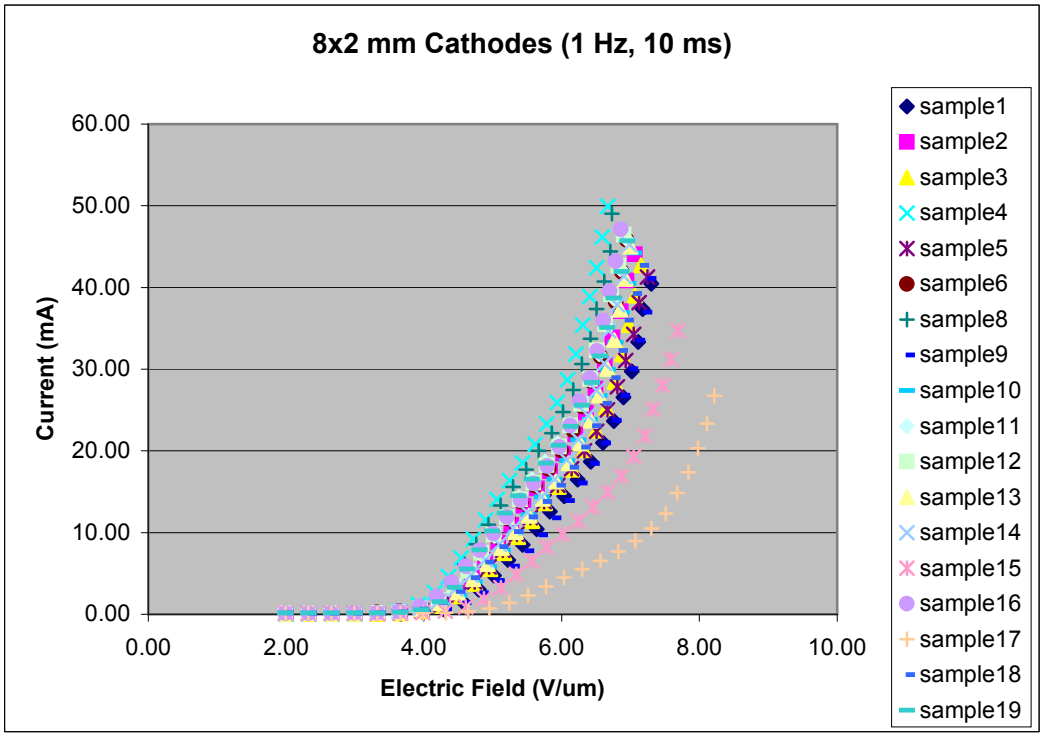

Figure 15: Current vs. electric field for eighteen samples in second batch of cathodes

4.2 Lifetime Measurements

Diode lifetime measurements were done to evaluate the performance of the cathodes. Prior to the test, diode field emission measurement was obtained again using 1 % duty cycle (1 Hz, 10 ms) and 150 μm gap distance since the cathodes had been left in a dessicator for about eight months. Figure 16 shows the field emission for sample 11 from the first batch of cathodes and how the cathode has degraded over time. Sample 11 was chosen because it still had good field emission. The same current can still be obtained but at a higher gate voltage since the turn-on field has increased by ~2 V/μm. The cathode degradation can be attributed to oxidation of the cathode and can normally be reversed by baking the chamber to a high temperature. However, the chamber could not be baked to a very high temperature because there were plastic parts used in the assembly that limited the baking temperature.

For this test, the chamber was baked overnight and the vacuum reached 1.4×10^{-7} Torr. The parameters used for the test was 1 % duty cycle (1 Hz, 10 ms), 10 kΩ resistance, and 150 μm gap distance between cathode and gate. The target cathode current was 25 mA. Figure 17 shows that the current is able to remain constant at 25 mA over the duration of the test, which was over a day. The voltage only changed by ~100 V from 1450 V to ~1550 V in order to maintain the target current. Figure 18 shows the same test done but at 10% duty cycle (1 Hz, 100 ms). The vacuum was at 7.7×10^{-8} Torr. From the plot of voltage vs. time, it can be seen that the voltage increases linearly after a period of time to maintain the target current but the increase is not extremely large, only ~200 V. This is caused by the degradation of the cathode, which could be reversed if the chamber was baked to a much higher temperature prior to the test, well over 100 °C.

.

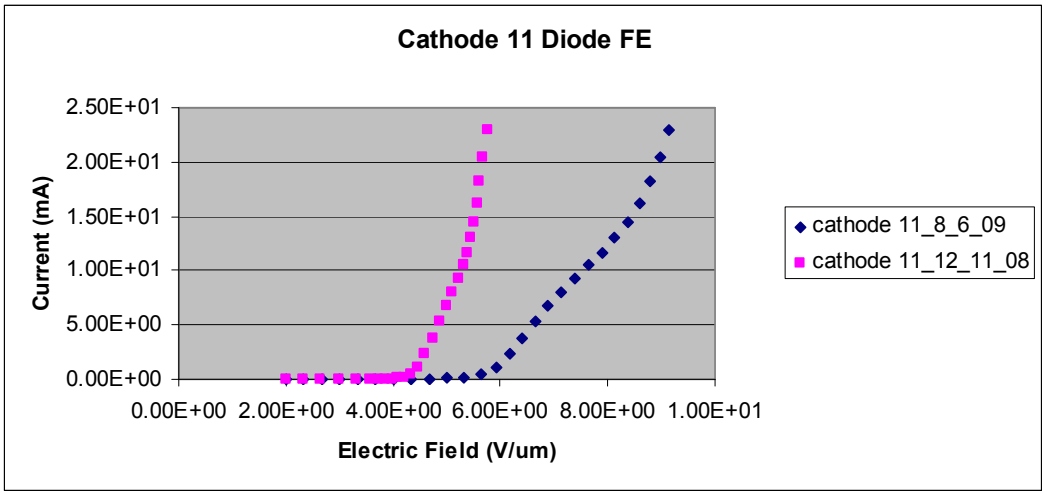

Figure 16: Current vs. electric field for sample 11 at two different periods of time

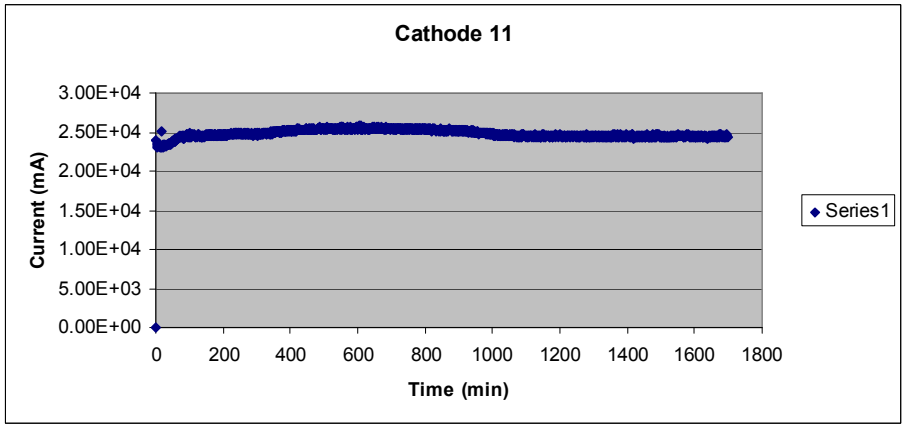

(a)

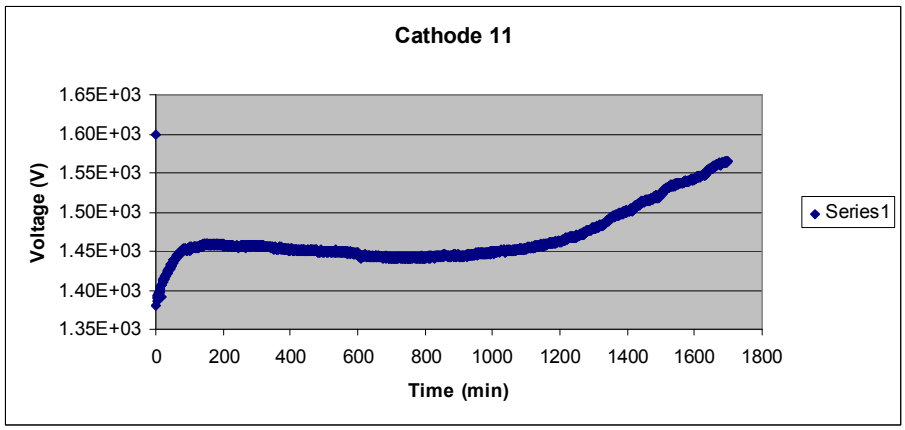

(b)

Figure 17: (a) Current vs. time; and (b) voltage vs. time at 1% duty cycle

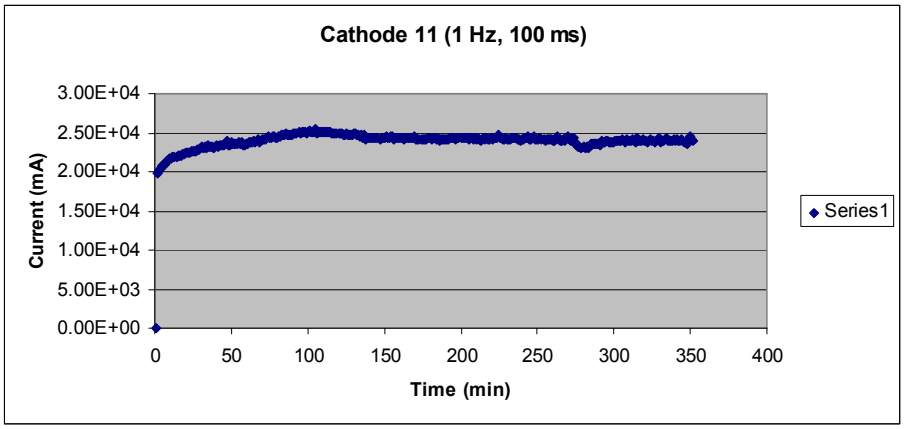

(a)

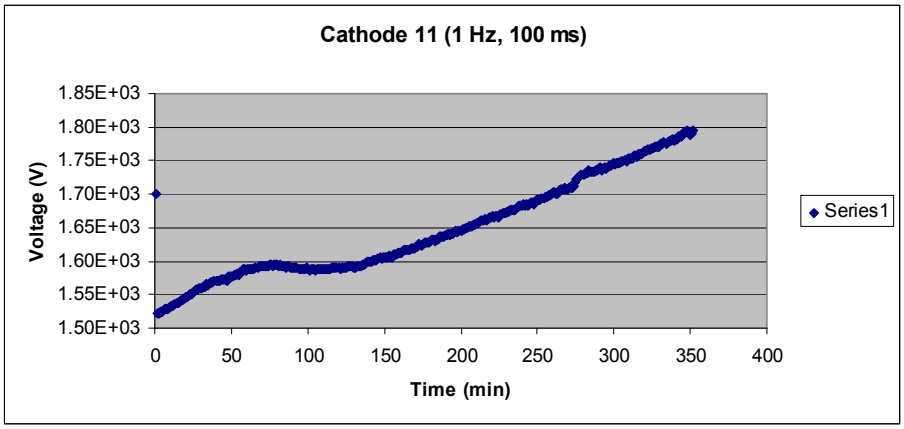

(b)

Figure 18: (a) Current vs. time; and (b) voltage vs. time at 10% duty cycle

4.3 Initial Results for quasi-monochromatic imaging

Quasi-monochromatic or narrow energy band imaging has several advantages for DBT. Among the advantages of quasi-monochromatic imaging are reduced dose to the patient, increased contrast between tissues of similar attenuation (i.e. masses and soft tissue), and a lower false positive rate due to the increase in image contrast. However, the main disadvantage is a reduction in flux.[12] Using a large pixel area to acquire a higher cathode current compensates for the loss of flux. Moreover, the total scan time will have to be longer to compensate for the reduction in flux.

From simulated data, we have shown that it is possible to achieve a reasonable scan time using a 100th VL Ce filter. To confirm the simulation, an experiment was conducted using our CNT-based single source micro-CT scanner with a W anode and 200 μm thick Be window to generate the x-rays and an XR-100T CdTe x-ray detector from Amptek to measure the x-ray spectra with and without Ce filtration. Ce was chosen as the filter due to its ability to filter out high-energy photons above its K-edge of 40.4 keV. [12] The detector had a 200 μm in diameter W collimator that is 2 mm thick attached to it. The source-to-detector distance was 64.5 cm, which is the same as the source-to-object distance used for the stationary DBT system. The gate, first focusing electrode, and second focusing electrode voltages were set at 1000 V, 800 V, and 2.6 kV, respectively. The transmission rate for the electron source was 55% and a 10% duty cycle (1 Hz, 100 ms) was used. Since the cathode current fluctuates slightly, it was manually recorded every 15 s for measurements lasting 100 s and every 100 s for measurements lasting 500 s or 1000 s and averaged. The different cases tested were a 0.768 mm Al filter at 30 kV, an Al/50th VL Ce filter and an Al/100th VL Ce filter at 60 kV. The 50th VL Ce has a thickness of 0.651 mm and the 100th VL Ce has a

thickness of 0.766 mm. The attenuation coefficient at 32 kV was used to calculate the thickness of the Ce filters and is about the same as the attenuation coefficent at 60 kV. Since Ce reacts with air, the filters were encased between two acrylic plates each 3.3 mm thick with grooves for two o-rings so that it would not be exposed to air (Fig. 19). Prior to obtaining the spectra, a W spectrum with no filtration at 60 kV and known peaks was recorded and used to calibrate the other spectra (Fig. 20). Figure 21 shows the experimental W spectra after processing and figure 22 shows the simulated W spectra generated using SRS-78 Spectrum Processor. The plots of the spectra with cerium filtration are magnified by a factor of five. The shapes of the experimental W spectra are consistent with the simulated spectra except for the photons seen in the lower energies that should have been filtered. This can be explained by the escape events that occur in the CdTe detector. Photons with incident energy just above the K-edges of Cd and Te, which are 26.7 keV and 31.8 keV, respectively, undergo photoelectric interactions, leaving the Cd and Te atoms in an excited state. When the atoms transition to ground level, they emit characteristic x-ray in which either the energy is fully deposited onto the detector or if the incident energy is greater than the K-edges, can lead to escape events at lower energies. [13]

Several trials were done for each case and the results of the different trials were averaged. The total scan time to achieve the same number of total photons assuming a target of 52 mA/pixel and 80 mA-s total for the stationary DBT system for W/Al at 30 kV, W/Al/Ce 50th VL, and W/Al/Ce 100th VL at 60 kV are 1.54 s, 8.69 s, 12.1 s, respectively. Table 1 summarizes the total scan time. Compared to the total scan time for the Siemens Mammomat Novation of 20 s for 25 views in full-resolution mode, a reasonable scan time when a 50th VL or 100th VL of Ce filter is used can be achieved. [11]

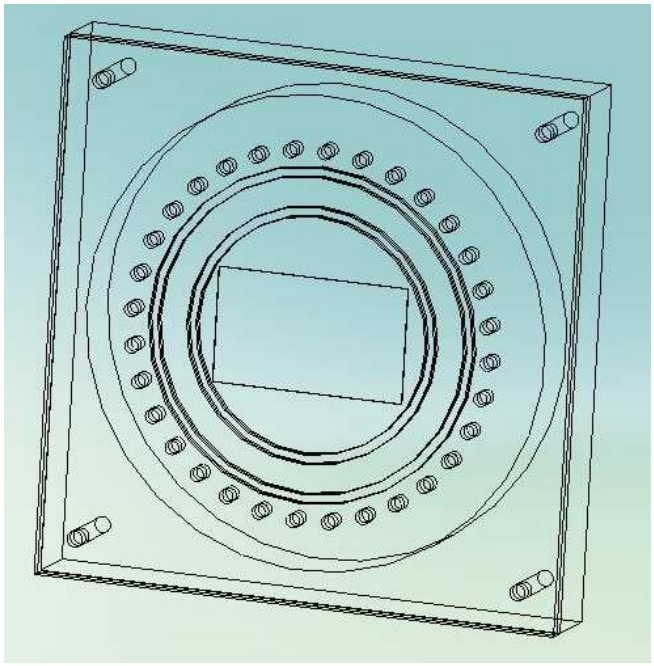

Figure 19: Wireframe view of Ce filter enclosure

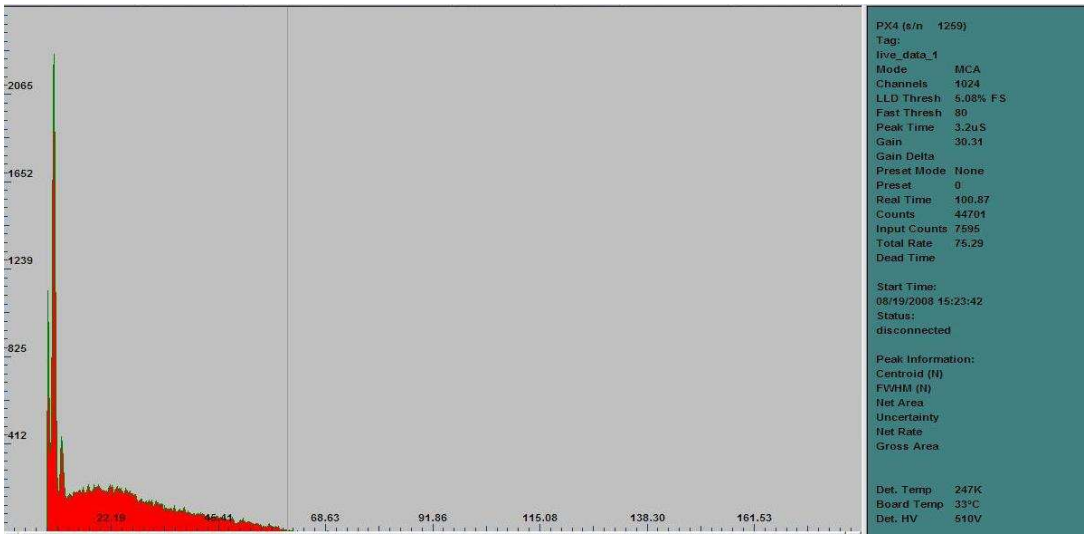

Figure 20: W spectrum at 60 kV with no filtration used for calibration

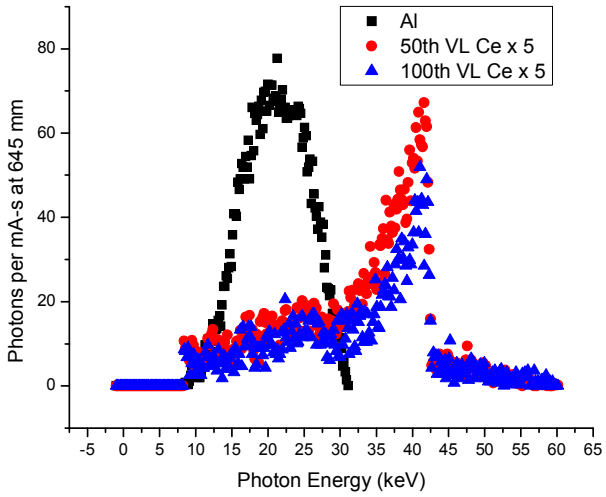

Figure 21: Experimental W spectra with Al filter at 30 kV, Al/50th VL Ce filter and Al/100th VL Ce filter at 60 kV and magnified by a factor of five

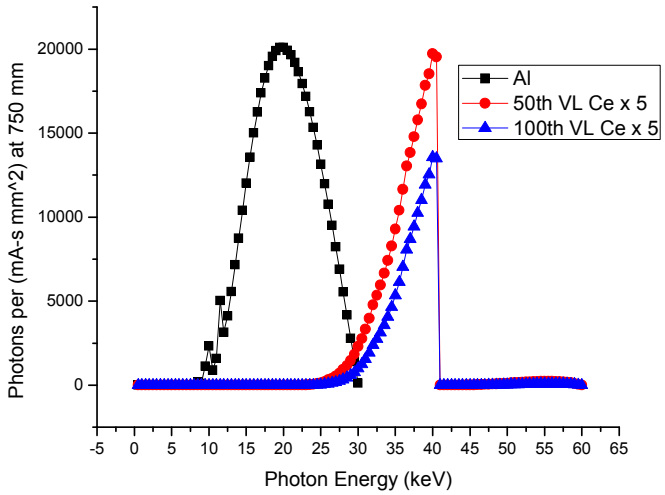

Figure 22: Simulated W spectra with Al filter at 30 kV, Al/50th VL Ce filter and Al/100th VL Ce filter at 60 kV and magnified by a factor of five

Table 1. Photons per mA-s at 645 mm, relative photon flux, mA-s/view, total mA-s, and total scan time for three filter conditions.

Anode/Filter(s) (energy)	Photons per mA-s at ~645 mm	Relative Photon Flux	mA-s/view	Total mA-s	Total Scan Time (s)
W/Al (30 kV)	4725	1	3.2	80	1.54
W/Al/Ce-50th VL (60 kV)	837	0.177	18.1	452	8.69
W/Al/Ce-100th VL (60 kV)	603	0.128	25.1	627	12.1

CHAPTER 5

CONCLUSION

Although many improvements have been made to the design of the system, further improvements can still be made. Most of these would require having most of the components machined again so they have not been implemented. The most critical improvement is to change the design of the anode holder. The current design depends a great deal on the accuracy of the machining. Tungsten is more difficult to machine than molybdenum, a metal commonly used for the anode. Thus, when the anode is not accurately machined to fit the holder, it is susceptible to falling out of it, especially during the baking process where it is subjected to temperature changes.

Another improvement that can be made is to eliminate the counterbores that are used to fix the components to the Al base. Due to the myriad parts in the system, assembly is a tedious process. The counterbores make it more tedious and difficult because of the need for two people to assemble each pixel. One person needs to hold all four screws for each pixel in place while the other person does the assembly. It is also problematic because if part of the ceramic screws break, it tends to get lodged in the threaded hole in the second focusing electrode and would need to be drilled out in order to remove it. The purpose of using the counterbores is to hide the screw heads to prevent arcing. However, this can be achieved with countersinks. To further facilitate the assembly process, the number of parts and connections used can be reduced by making most of the electrodes single pieces instead of twenty-five separate pieces for each pixel. The gates, focusing units, and anodes are all held

at the same potential. Thus, the gates for the pixels can be grouped together. This applies to the focusing units and anodes as well. It would be more difficult to machine a single piece to connect all twenty-five pixels, especially since each pixel is positioned at an angle so that the x-ray beam hits the center of the object. Instead, they can be divided in units with each unit connecting five pixels. By using fewer components, the number of connections that have to be made is minimized so the chamber will be less crowded.

Yet another improvement that can be made is to change the anode spacer. The current design has two threaded holes, one to attach the anode holder to the spacer and the other to attach the anode spacer to the Al base. The problem with using threaded holes is that it is very easy for parts of the ceramic pieces to break when removing the screws. Sometimes, it is enough to change the height of the spacer. This can partially be corrected for by adding washers to maintain the same height if necessary. However, if the design for the Al base could be changed, a better design would be to use clear holes for the anode spacer and a single vented stainless steel screw to attach all three pieces together. Instead of the threads for the screws being in the spacer, it would be in the Al base.

The method to separate the cathode from the gate can also be improved. To achieve the required thickness of 180 μm for the gap distance between cathode and gate, a thicker mica sheet is peeled one layer at a time. Not only is it difficult to peel mica sheets and get the same thickness for all of them, the thickness is also not uniform over a single mica sheet. Moreover, mica is not a good material to use in vacuum. A possible solution would be to use something more uniform and solid such as glass. The disadvantage is that such a thin piece of glass is difficult and expensive to etch to fit the design. It may also be too fragile and might break from the pressure applied to it.

Future work for this system involves fully characterizing the system including performing triode field emission measurement, FSS measurement, geometry calibration, and MTF measurement. The system will be used with a Hologic detector. Once operation at 30 kV is successful, operation at 60 kV and quasi-monochromatic imaging will be tested. Quasi-monochromatic imaging will be implemented using a 50^{th} VL and 100^{th} VL Ce filter in order to increase contrast between tissues of similar attenuation and reduce patient dose.

REFERENCES

1. American Cancer Society [Internet]. Atlanta (GA): The Society; c2010. How many women get breast cancer; 29 Sep 2009 [cited 2010 Mar 18]; [1 screen]. Available from: http://www.cancer.org/docroot/CRI/content/CRI_2_2_1X_How_many_people_get_breast_cancer_5.asp?sitearea=

2. Gold RH, Bassett LW, Widoff BE. Highlights from the history of mammography. Radiographics 1990;10(6):1111-31.

3. Iniewski K. Medical imaging: principles, detectors, and electronics. Hoboken (NJ): John Wiley and Sons; 2009.

4. Bharath AA. Introductory medical imaging (synthesis lectures on biomedical engineering). San Rafael (CA): Morgan & Claypool; 2008.

5. Lewin JM, D'Orsi CJ, Hendrick RE, Moss LJ, Isaacs PK, Karellas A, Cutter GR. Clinical comparison of full-field digital mammography and screen-film mammography for detection of breast cancer. AJR Am J Roentgenol 2002;179(3):671-7.

6. Pisano ED, Yaffe MJ, Kuzmiak CM. Digital mammography. Philadelphia: Lippincott Williams & Wilkins; 2004.

7. Peart, O. Mammography and breast imaging: just the facts. Kingsport (TN): McGraw-Hill; 2005.

8. Smith, A. Fundamentals of breast tomosynthesis: improving the performance of mammography. Hologic Inc; 2008.

9. Wang S, Zhou O, Chang S. Carbon-nanotube field emission electron and x-ray technology for medical research and clinical applications. In: Narlikar AV, Fu YY, editors. Oxford handbook of nanoscience and technology. Vol. 3. New York: Oxford University Press; 2010. p. 674-699.

10. Meyyappan, M. Carbon nanotubes: science and applications. Boca Raton (FL): CRC Press; 2004.

11. Yang G et al. Stationary digital breast tomosynthesis system with a multi-beam field emission x-ray source array. In: SPIE proceeding on medical imaging; 2008.

12. Crotty DJ, McKinley RL, Tornai MP. Experimental spectral measurements of heavy K-edge filtered beams for x-ray computed mammotomography. Phys Med Biol 2007; 52:603-616.

13. Redus R. CdTe measurement of x-ray tube spectra: escape events. In: Amptek [Internet]. Bedford (MA): Amptek; 22 Apr 2008 [cited 2010 Mar 28]. Available from: http://id3456.securedata.net/amptek/epeaks.html